Published in final edited form as:
Dev Cell. 2012 September 11; 23(3): 560–572. doi:10.1016/j.devcel.2012.08.008.

PKD Controls αvβ3 Integrin Recycling and Tumor Cell Invasive Migration Through its Substrate Rabaptin-5

Claudine Christoforides[1,*], **Elena Rainero**[2,*], **Kristin K. Brown**[1], **Jim C. Norman**[2,#], and **Alex Toker**[1,#]

[1]Department of Pathology, Beth Israel Deaconess Medical Center, Harvard Medical School, Boston, MA, 02215

[2]Beatson Institute for Cancer Research, Glasgow, United Kingdom

Summary

Integrin recycling is critical for cell migration. Protein Kinase D (PKD) mediates signals from the platelet-derived growth factor-receptor (PDGF-R) to control αvβ3 integrin recycling. We now show that Rabaptin-5, a Rab5 effector in endosomal membrane fusion, is a PKD substrate. PKD phosphorylates Rabaptin-5 at Ser407 and this is both necessary and sufficient for PDGF-dependent short-loop recycling of αvβ3, which in turn inhibits α5β1 integrin recycling. Rab4, but not Rab5, interacts with phosphorylated Rabaptin-5 toward the front of migrating cells to promote delivery of αvβ3 to the leading edge, thereby driving persistent cell motility and invasion that is dependent on this integrin. Consistently, disruption of Rabaptin-5 Ser407 phosphorylation reduces persistent cell migration in 2D and αvβ3-dependent invasion. Conversely, invasive migration that is dependent on α5β1 integrin is promoted by disrupting Rabaptin phosphorylation. These findings demonstrate that the PKD pathway couples receptor tyrosine kinase signaling to an integrin switch, via Rabaptin-5 phosphorylation.

Introduction

The regulated recycling of integrins is required for efficient cell migration (Jones et al., 2006; Mai et al., 2011; Pellinen et al., 2006; Pellinen and Ivaska, 2006; Ramsay et al., 2007; Shattil et al., 2010). Inhibition of SNARE-mediated membrane traffic by tetanus toxin or inhibition of N-ethylmaleimide-sensitive fusion protein (NSF) opposes β1 integrin recycling, and reduces cell spreading and migration (Skalski and Coppolino, 2005). Two distinct integrin recycling pathways control cell migration: the small GTPases Rab11 and Rab4 regulate long- and short-loop recycling, respectively. Disruption of long-loop recycling by blocking Rab11 function inhibits invasive migration (Fan et al., 2004; Powelka et al., 2004; Yoon et al., 2005). Rab4 is instead required for PDGF-stimulated αvβ3 recycling and cell adhesion and spreading (Roberts et al., 2001; White et al., 2007).

[#]Correspondence: atoker@bidmc.harvard.edu, j.norman@beatson.gla.ac.uk.
[*]Equal contribution

Supplemental Information
Supplemental Information includes experimental procedures, three figures and two movies and can be found with this article online at doi:

Protein Kinase D (PKD) has been shown to control Rab4-dependent αvβ3 integrin recycling to regulate cell motility (Woods et al., 2004). PKD comprises a family of three mammalian serine/threonine protein kinases in the calcium/calmodulin-dependent protein kinase family (Rykx et al., 2003). In the canonical pathway of PKD activation, growth factor signals are transduced through receptor tyrosine kinases to activate phospholipase C-γ (PLC-γ). PLC-γ cleaves phosphatidylinositol 4,5-bisphosphate (PIP $_2$) to produce inositol 1,4,5-triphosphate (IP_3) and diacylglycerol (DAG). DAG recruits cytosolic PKD to the plasma or Golgi membranes, co-localizing it with its upstream kinase PKC (Protein Kinase C) (Zugaza et al., 1996). The binding of DAG to the PKD cysteine-rich domains facilitates phosphorylation of the PKD activation loop residues by PKC, leading to kinase activation. A number of substrates have been identified that mediate the PKD signal to numerous cellular responses, including proliferation, survival, and vesicle trafficking from the Golgi. PKD is a basophilic kinase and phosphorylates the optimal consensus phosphorylation motif LXXRXs/t (where X represents any amino acid). PKD substrates that contain this motif include class II histone deacetylases (HDACs (Vega et al., 2004)), phosphoinositide 4-kinase IIIβ (PI4KIIIβ (Hausser et al., 2005)), heat shock protein 27 (Hsp27, (Doppler et al., 2005)) and the lipid transport proteins CERT (ceramide transfer protein, (Fugmann et al., 2007)) and OSBP (oxysterol binding protein, (Nhek et al., 2010)).

The interaction between PKD and αvβ3 is required for PDGF-driven, Rab4-dependent integrin recycling, and in turn cell migration (Woods et al., 2004). Recycling of αvβ3 can impact cell migration by inhibiting α5β1 and EGFR recycling and their ability to signal to Rho and Akt/PKB, respectively (Caswell et al., 2008; Vukmirica et al., 2006; White et al., 2007). However, the signaling intermediates and substrates of PKD that modulate integrin recycling and cell migration have not been identified.

Rabaptin-5 is an essential Rab5 effector with amino-terminal Rab4 and carboxyl-terminal Rab5-binding domains (Stenmark et al., 1995; Vitale et al., 1998). Rabaptin-5 forms a complex with Rabex-5, a Rab5 guanine nucleotide exchange factor. Rabaptin-5 binds Rab5-GTP and promotes co-localization of Rab5 with Rabex-5. This in turn stabilizes Rab5-GTP leading to endosomal membrane fusion during endocytosis, such that Rabaptin-5 overexpression results in enlarged endosomal vesicles while its immunodepletion blocks Rab-5 dependent endosome formation (Stenmark et al., 1995). Rabaptin-5 also couples to Rab4 and Gamma1 adaptin on recycling endosomes to regulate receptor recycling (Deneka et al., 2003).

Here we report that Rabaptin-5 is a substrate of PKD. PKD phosphorylates Rabaptin-5 at Ser407, and this controls αvβ3 and α5β1 integrin and EGFR recycling. In turn, this pathway regulates the morphology and speed of migrating cells in 2D and 3D.

Results

PKD phosphorylates Rabaptin-5 at Ser407 In Vitro and in Cells

Phosphoproteomic screens have identified phosphorylation of Rabaptin-5 at Ser407 in a consensus sequence that conforms to the optimal PKD phosphorylation motif (LXRXXs/t) (Dephoure et al., 2008; Villen et al., 2007). The PKD consensus motif surrounding Ser407 is conserved in mammals and other species including fish, flies and worms (Figure 1A). A distinct putative PKD consensus phosphorylation motif on Rabaptin-5 is also found at Ser162, although to date no phosphopeptides with this sequence have been mapped by functional proteomics. To determine whether Rabaptin-5 is a PKD substrate, we first stimulated NIH-3T3 cells with platelet-derived growth factor (PDGF) to activate PKD. Endogenous Rabaptin-5 was immunoprecipitated and immunoblotted with an antibody that recognizes the PKD consensus phosphorylation motif, anti-PKD pMOTIF (Doppler et al.,

2005). The reactivity between Rabaptin-5 and the PKD pMOTIF antibody increases over time upon PKD activation by PDGF, and is attenuated by pre-treatment with Gö6976, a PKC/PKD inhibitor (Figure 1B). Phosphorylation of PKD at pS916 serves as an indicator of PKD activation. Next, to determine if PKD is exclusively required for phosphorylation of endogenous Rabaptin-5, short hairpin RNA (shRNA) was used. In control cells, PDGF stimulates Rabaptin-5 phosphorylation, whereas in PKD knockdown cells, this is abrogated (Figure 1C). Taken together, these data show that PKD promotes Rabaptin-5 phosphorylation during PDGF-initiated signal relay.

PKD phosphorylates Rabaptin-5 at Ser407, since expression of constitutively active PKD in cells induces phosphorylation of wild type Rabaptin-5, but not a Ser407Ala mutant (Figure 1D). In an *in vitro* kinase assay, purified PKD directly phosphorylates Rabaptin-5 isolated by immunoprecipitation from cells expressing Myc-Rabaptin-5. Importantly, Rabaptin-5 Ser407Ala is not phosphorylated by PKD in this assay (Figure 1E). Therefore, PKD directly phosphorylates Rabaptin-5 at Ser407. Since the PKD pMOTIF antibody is not immunoreactive towards Rabaptin-5 Ser407Ala in cells expressing activated PKD (Figure 1D), and there is no appreciable phosphorylation of Rabaptin-5 Ser407Ala by PKD in an *in vitro* kinase assay using $\gamma[^{32}P]$-ATP (Figure 1E), this implies that Ser162 is not phosphorylated by PKD. Moreover, Ser162 phosphorylation has not been detected in the same phosphoproteomic analyses that have identified Ser407 phosphorylation (Dephoure et al., 2008; Villen et al., 2007). While we cannot formally rule out Ser162 phosphorylation, we conclude that PKD exclusively phosphorylates Rabaptin-5 at Ser407.

Rabaptin-5 phosphorylation controls αvβ3 and α5β1 integrin recycling

Since PKD controls integrin recycling downstream of Rab4 (Woods et al., 2004), and Rabaptin-5 is a Rab4 effector (Vitale et al., 1998), we reasoned that phosphorylation of Rabaptin-5 at Ser407 by PKD may control integrin recycling. NIH-3T3 fibroblasts were surface labelled and internalization allowed to proceed for 15 min at 22°C to allow receptors to accumulate in Rab4-positive early endosomes, and recycling of both the endogenous mouse αvβ3 integrin (Figure 2A; left hand bars and Figure 2B) and the exogenously-expressed human αvβ3 heterodimer (Figure 2A; right hand bars) back to the plasma membrane was determined in the presence and absence of PDGF, as described previously (Roberts et al., 2001). In the absence of growth factor, αvβ3 recycling is slow, and addition of PDGF greatly enhances the rate at which αvβ3 returns to the plasma membrane (Figure 2B). Silencing of Rabaptin-5 using small interfering RNA (siRNA) blocks the ability of PDGF to initiate recycling of αvβ3 (compare white and yellow bars, Figure 2A). However, Rabaptin-5 knockdown also appears to increase basal integrin recycling. This can likely be attributed to a decrease in the internalization of αvβ3 (see below), as Rabaptin-5 is a critical Rab5 effector in endocytosis. To determine a requirement for PKD phosphorylation of Rabaptin-5 in PDGF-dependent integrin recycling, we used Rabaptin-5 Ser407 mutants that are resistant to silencing. Expression of wild-type Rabaptin-5 restores PDGF-regulated αvβ3 recycling (red bars and red curve, Figure 2A, B), whereas expression of Rabaptin-5 Ser407Ala blocks the ability of PDGF to stimulate recycling (green bars and green curve). Moreover, the phosphomimetic mutant Ser407Asp promotes recycling in the absence of PDGF stimulation (grey bars, Figure 2A). Similar results are obtained in cells transduced with Rabaptin-5 shRNA, WT and Ser407Ala rescue mutants when the recycling of co-transfected human αvβ3 was measured (Figure 2A; red and green bars, hαvβ3). A Rabaptin-5 Ser162Ala mutant rescues recycling to the same extent as wild-type, providing further evidence that Ser162 is not regulated by PKD signaling (Figure 2A, blue bars). Therefore, Rabaptin-5 Ser407 phosphorylation is both necessary and sufficient to regulate PDGF-dependent αvβ3 integrin recycling.

Since Rabaptin-5 is an essential effector of Rab5 in endocytosis (Stenmark et al., 1995), we next evaluated whether the recycling defect in cells expressing Rabaptin-5 Ser407Ala is due to impaired internalization. As expected, knockdown of Rabaptin-5 with siRNA results in impaired internalization of αvβ3 integrin (Figure 2C, yellow curve). Re-expression of either wild-type Rabaptin-5 or Ser407Ala mutants that are resistant to silencing rescues this phenotype (Figure 2C, red and green curves), indicating that the regulation of integrin recycling by Rabaptin-5 phosphorylation at Ser407 is not due to a defect in internalization. Cell lysates from Figures 2A and 2B were immunoblotted with a Rabaptin-5 antibody to confirm knockdown and expression of non-silenceable mutants (Figure 2D).

It is now clear that some of the influence of αvβ3 on cell migration is mediated by its ability to negatively modulate the trafficking of other receptors. For instance when αvβ3 recycling is rapid, α5β1 returns slowly to the plasma membrane and cells move persistently. However, when αvβ3 trafficking (or its ligand engagement) is compromised this leads to increased recycling of α5β1 which blocks persistent migration and promotes an elongated cellular morphology that effectively increases the speed of motility (Caswell et al., 2008; White et al., 2007). Furthermore, the cross-talk between αvβ3 and α5β1 trafficking is mediated by the Rab11 effector, Rab Coupling Protein (RCP) which not only is responsible for increased α5β1 recycling, but also acts to link α5β1 and EGFR such that the trafficking of these two receptors is physically coordinated (Caswell et al., 2008). It is the signaling consequences of these trafficking interactions, such as increased signaling of α5β1 to Rho effectors and the enhancement of the ability of EGFR1 to activate Akt, that implement alterations in cell migration. We therefore tested the contribution of Rabaptin-5 phosphorylation at Ser407 by PKD to α5β1 and EGFR recycling. In cells transfected with Rabaptin-5 siRNA, re-expression of Rabaptin-5 Ser407Ala enhances α5β1 recycling compared to wild-type Rabaptin-5, in both NIH-3T3 fibroblasts (Figure 3A) as well as A2780 ovarian carcinoma cells (Figure 3B). This increase is not due to altered α5β1 internalization (Figure 3C). Moreover, Rabaptin-5 Ser407Ala also promotes EGFR recycling compared to wild-type Rabaptin-5 (Figure 3D). The PKD-Rabaptin-5 signaling pathway therefore regulates the recycling of αvβ3 integrin, α5β1 integrin and EGFR.

Rabaptin-5 phosphorylation regulates persistent directional migration

Increased αvβ3 and reduced α5β1 recycling promote the directional and persistent migration of fibroblasts on 2D surfaces (White et al., 2007). To determine the contribution of Rabaptin-5 phosphorylation to cell migration, time-lapse images of NIH-3T3 cells expressing Rabaptin-5 mutants subsequent to Rabaptin-5 knockdown were collected. A monolayer was wounded, individual cells migrating into the wound were followed and the persistence and speed of migration were extracted from the track plots (Figure 4A–D). Knockdown of Rabaptin-5 or PKD reduces persistent migration to a similar degree, and this is rescued by expression of siRNA-resistant wild type Rabaptin-5 (Figure 4A and 4B, and movie S1). In contrast, Rabaptin-5 Ser407Ala is completely unable to rescue persistent migration of NIH-3T3 fibroblasts. A requirement for Rabaptin-5 in directional migration is also demonstrated by an impairment in the overall Forward Migration Index (FMI) of cells expressing Ser407Ala compared to cells expressing wild-type Rabaptin-5 (Figure 4C). We have previously shown that reduced persistent cell migration is commonly accompanied by increased migration speed, which is also a consequence of enhanced α5β1 recycling (White et al., 2007). Consistent with this, silencing of Rabaptin-5 increases migration speed in a way that is reversed by re-expression of wild-type Rabaptin-5, but not Rabaptin-5 Ser407Ala (Figure 4D).

PKD is responsible for trafficking αvβ3 integrin to nascent adhesions (Woods et al., 2004). To determine the role played by phosphorylation of Rabaptin-5 by PKD in recruitment of αvβ3 to the cell front, which is where new focal adhesions are formed, we used a GFP-

tagged β3 integrin (Figure 4E). Using this approach we quantified the proportion of αvβ3 present within new adhesions at the cell front with respect to αvβ3 that is located further back in the cell (Figure 4F). In both control cells and Rabaptin-5 knockdown cells in which wild-type Rabaptin-5 has been re-expressed, approximately 70% of αvβ3 is present primarily within adhesive structures that are localized to a tight band within 2.5 μm of the advancing cell front (Figure 4E,F). Knockdown of PKD1 or expression of Rabaptin-5 Ser407Ala leads to a significant reduction of αvβ3 at the cell front, and a commensurate increase in the quantity of the integrin in larger adhesions nearer to the cell rear (Figure 4E,F).

Taken together, these data indicate that Rabaptin-5 phosphorylation at Ser407 is required for delivery of αvβ3 to newly forming adhesions at the front of migrating cells, and the ability of this integrin to support persistent cell migration on 2D surfaces.

Rabaptin-5 controls integrin recycling and PDGF-driven migration through Rab4

Since phosphorylation of Rabaptin-5 by PKD is required for the proper execution of Rab4-dependent events, such as αvβ3 recycling and its delivery to the cell front during cell migration, we evaluated how this phosphorylation influences the spatial relationship and physical association between Rabaptin-5 and the GTPase in migrating cells. We first determined the consequences of expressing Cherry-tagged Rab4 and Rab5 on cell migration. Expression of Cherry-Rab4 does not alter the way in which cells migrate into scratch-wounds, nor does it affect the ability of Rabaptin-5 Ser407Ala to decrease persistence and increase migration speed (Figure 5A). By contrast, expression of Cherry-Rab5 alters both the migratory persistence and forward migration index (FMI) of cells expressing wild type Rabaptin-5, and suppresses the ability of mutant Rabaptin-5 to influence migratory persistence and speed (Figure 5A). The absence of any effect of Cherry-Rab4 overexpression on cell migration renders it a useful tool in the context of experiments designed to probe the contribution of the Rabaptin-5/Rab4 complex on cell migration. However, the same argument cannot be invoked for overexpression of Cherry-Rab5.

We expressed Cherry-Rab4 in combination with either GFP-Rabaptin-5 or GFP-Rabaptin-5 Ser407Ala and used fluorescence live cell imaging to evaluate the distribution of these proteins in both control and PKD knockdown cells as they migrated into scratch-wounds. Rabaptin-5 and Rab4 are localized to vesicles positioned in front of the nucleus with respect to the direction of cell migration (Figure 5B; Figure S1 and movie S2). We quantified this by developing an algorithm to determine the proportion of fluorescent Rabaptin-5 or Rab4 that is localized within the anterior portion of the cell. Moreover, we quantitatively assessed the degree to which Rabaptin-5 and Rab4 co-localize in migrating cells. In cells expressing wild-type Rabaptin-5, more than 80% of cellular Rab4 and Rabaptin-5 are located in the perinuclear region anterior to the direction of migration, and these two proteins co-localize very closely (Figures 5C–F). Expression of Rabaptin-5 Ser407Ala, or knockdown of PKD1 ablates the ability of Rabaptin-5 and Rab4 to position themselves at the cell front, and significantly reduces co-localization between the two proteins (Figures 5B–F; Figure S1 and movie S2). Furthermore, the influence of Rabaptin-5 phosphorylation on co-localization between Rabaptin-5 and Rab4 is not evident in cells that are distant from the wound's edge (Figures S2A,B), indicating that PKD1 can only influence Rabaptin-5/Rab4 association in migrating cells.

We next determined the association between Rabaptin-5 and Rab4 by immunoprecipitating myc-Rabaptin-5 (or myc-Rabaptin-5 mutants) and assessing the amount of co-precipitating GTPase by immunoblotting. To ensure that the cells were migrating at the time of lysis, we performed these experiments on cells that had been plated onto fibronectin-coated surfaces at low density and treated with PDGF for 1 hr. In migrating cells, the ability of Rab4 (Figure

5G) (but not Rab5 (Figure 5H)) to co-immunoprecipitate with Rabaptin-5 is reduced by mutation of Ser407 to Ala, or by siRNA of PKD1. Conversely, in cells that are confluent (and, therefore, not migrating) mutation of Ser407 to Ala, while enhancing an interaction with Rab5 (Figure S2F), has no effect on association of Rabaptin-5 with Rab4 (Figure S2E). Taken together, these data indicate that phosphorylation of Rabaptin-5 at Ser407 by PKD1 is necessary for tight association with Rab4, and the appropriate positioning of the Rabaptin-5/Rab4 complex as cells migrate into wounds. By contrast, this phosphorylation event does not influence Rabaptin-5/Rab4 association or colocalization in non-migrating cells.

Rabaptin-5's influence on tumor cell invasion is dependent on the ECM microenvironment

In addition to affecting a switch from persistent to random movement on 2D surfaces, integrin recycling influences invasive migration in 3D matrices (Caswell et al., 2008; Vukmirica et al., 2006). The contribution made by particular integrin heterodimers to invasion crucially depends on the availability of ECM ligands for those integrins. For instance, under circumstances where vitronectin (the main ligand for αvβ3) is abundant, but the concentration of fibronectin (the main ligand for α5β1) is low, invasion is strongly dependent on αvβ3. Indeed, when MDA-MB-231 breast cancer cells move into Matrigel in the presence of serum, but with no added fibronectin, their invasiveness is opposed by addition of c-RGDfV (a cyclic peptide that specifically blocks αvβ3) indicating that αvβ3 is required for invasion when fibronectin levels are low (Figure 6A). Moreover, silencing of Rabaptin-5 reduces invasion of MDA-MB-231 cells into Matrigel that does not contain fibronectin, and invasiveness is restored by re-expression of wild-type Rabaptin-5, but not Rabaptin Ser407Ala. However, when exogenous fibronectin is added to the Matrigel, the invasion of MDA-MB-231 (Figure 6B) and A2780 (Figure 6C) cells is not αvβ3-dependent. By contrast, in the presence of fibronectin, invasiveness becomes dependent on α5β1 and is actually enhanced by addition of cRGDfV (Figure 6B, C). This is due to a large compensatory increase in α5β1 trafficking that occurs following blockade of αvβ3, as previously shown (Caswell et al., 2008). Correspondingly, Rabaptin-5 silencing (which *promotes* α5β1 recycling) enhances MBA-MB-231 (Figure 6B) and A2780 (Figure 6C) cell migration into fibronectin-supplemented 3D Matrigel plugs, and this is reversed by expression of siRNA-resistant wild type Rabaptin-5, but not Ser407Ala mutant. Representative strips from the invasion assays are shown in Figure S3.

As well as being activated by αvβ3 inhibition, α5β1 recycling can be driven by mutant forms of the tumor suppressor p53 (Muller et al., 2009; Rainero et al., 2012). MDA-MB-231 cells express high levels of a DNA-binding domain p53 mutant (R280K) that has lost wild type activity, but which activates RCP-dependent α5β1 recycling and invasion (Muller et al., 2009). Thus the capacity of Rabaptin-5 knockdown to promote α5β1-dependent invasion in these cells is likely tempered by the ability of mutant p53 to drive this pathway. To test this model, we silenced Rabaptin-5 and mutant p53 (both alone and in combination) in MDA-MB-231 cells (Figure 6B). As reported previously (Muller et al., 2009), knockdown of mutant p53 reduces invasiveness of MDA-MB-231 cells into fibronectin-containing Matrigel (Figure 6B). However, when mutant p53 and Rabaptin-5 are knocked down in combination, MDA-MB-231 cells are highly invasive. Indeed, siRNA of Rabaptin-5 increases fibronectin-dependent invasiveness of MDA-MB-231 cells by ≈1.6-fold, but this is increased to ≈4.0-fold in mutant p53-knockdown cells. These data demonstrate that inhibition of Rabaptin-5 and expression of mutant p53 influence α5β1 trafficking and invasion at least in part by impinging on the same pathways. The type of α5β1-dependent invasive migration described above is commonly accompanied by the extension of long invasive pseudopods in the direction of migration when cells are plated onto 3D cell-derived matrices (Caswell et al., 2008; Caswell et al., 2007). When A2780 cells transfected with non-targeting siRNA (si-nt) are plated onto fibronectin-rich 3D cell-derived

matrices, they move with the slug-like morphology that is characteristic of cells that are recycling their α5β1 integrins slowly (Figure 6D). In contrast, knockdown of Rabaptin-5 results in the extension of long invasive pseudopods in the direction of migration. This phenotype is reversed in cells expressing wild-type siRNA-resistant Rabaptin-5, but not with Ser407Ala (Figure 6D). Pseudopod length was also measured and quantitated (Figure 6D). Collectively, these data demonstrate that control of integrin trafficking by PKD and Rabaptin-5 signaling modulates cellular morphology to favor either persistent or rapid/random movement. Furthermore, inhibition of this signaling pathway influences tumor cell invasion in a way that is dictated by the fibronectin content of the surrounding ECM microenvironment.

Discussion

Previous studies have demonstrated a role for PKD in the control of integrin recycling. PKD/Rab4 binding is required for PDGF-dependent recycling of αvβ3 integrin (Woods et al., 2004), and autophosphorylation of PKD at Ser916 is required for this interaction (White et al., 2007). More recently PKD phosphorylation at Ser916 has been shown to control αvβ3 internalization and recycling in endothelial cells in response to VEGF (di Blasio et al., 2010). Our data show that Rabaptin-5 is a PKD substrate that controls integrin recycling. Mutant Rabaptin-5 Ser407Ala blocks PDGF-stimulated αvβ3 short-loop recycling while phosphomimetic Rabaptin-5 Ser407Asp promotes recycling in the absence of PDGF (Figure 2A). Therefore, Rabaptin-5 phosphorylation by the PKD pathway is both necessary and sufficient to control endocytic trafficking of integrins. The regulated recycling of integrins requires a number of steps including vesicle internalization, docking to the sorting endosome, and delivery of recycling vesicles to the plasma membrane (Caswell et al., 2009). Growth factors initiate these steps (Gu et al., 2011), however to date only one signaling mechanism has been shown to connect signaling downstream of growth factors to integrin recycling, and this is phosphorylation of ACAP1 (a GAP for ARF6) by Akt which promotes its association with β1 integrin to stimulate recycling (Jackson et al., 2000; Li et al., 2005; Powelka et al., 2004). A phosphomimetic ACAP1 mutant induces β1 recycling in the absence of stimulation. Similarly, phosphomimetic Rabaptin-5 results in αvβ3 integrin recycling in the absence of growth factor stimulation (Figure 2A). PKD therefore has a dual function in the control of integrin recycling, by binding directly to αvβ3 and by signaling to Rabaptin-5 phosphorylation.

We propose a model in which the coordinated regulation of Rab5 and Rab4 by the PKD-Rabaptin-5 pathway controls the internalization and docking of αvβ3-containing vesicles and short-loop integrin recycling. This model is supported by the finding that Rabaptin-5 regulates the internalization of αvβ3, a Rab5-dependent process. Indeed, silencing of Rabaptin-5 decreases endocytosis of αvβ3 integrin (Figure 2C) and this is restored to control levels by re-expression of either wild-type Rabaptin-5 or its Ser407Ala mutant. This is consistent with our data indicating that Rabaptin-5 phosphorylation does not influence its association with Rab5 in migrating cells. However, Rabaptin-5 phosphorylation by PKD at Ser407 controls both its association with Rab4 and the localization of the Rabaptin-5/Rab4 complex to the front portion of migrating cells (Figure 5), which, in turn, properly direct integrin trafficking to nascent focal adhesions at the cell front to support persistent cell migration. Notably, the association of phosphorylated Rabaptin-5 and Rab4 is only observed in migrating cells (Figures 5 and S2), highlighting the importance of the spatio-temporal control of Rab4 by Rabaptin-5 phosphorylation towards persistent movement. Since Rab4 activity is required for αvβ3 recycling (Roberts et al., 2001; van der Sluijs et al., 2001) and phosphorylated Rabaptin-5 preferentially binds to Rab4 over Rab5, it is possible that Rabaptin-5 phosphorylation stimulates Rab4 GTP-loading. Rabaptin-5 phosphorylation may thus function simply to increase the quantity of active Rab4 within the cell. However, we are

unable to restore persistent migration in Rabaptin-5 Ser407Ala-expressing cells by overexpressing Cherry-Rab4 (Figure 5A) or the constitutively active Gln67Leu mutant of Rab4 (not shown), indicating that Rabaptin-5 phosphorylation doesn't simply act by increasing Rab4 GTP-loading, but by coordinating the localization of activated Rab4 to endosomal domains that are involved in αvβ3 recycling. And PKD may be concomitantly recruited to such an endosomal subdomain by its association with the β3 integrin cytotail, thus ensuring that Rabaptin-5 phosphorylation and, in turn, Rab4 recruitment occurs in the appropriate place for returning integrins to the cell front. Interestingly, a kinase inactive mutant of PKD binds not only to αvβ3 (Woods et al., 2004) but also to Rab4 (A.T. and C.C., unpublished results), suggesting that an endosomal signaling complex containing αvβ3, Rab4, PKD, and Rabaptin-5 coordinates the spatio-temporal regulation of short-loop integrin recycling.

There is some disagreement in the literature as to the role played by PKD in cancer cell invasion. Whilst some studies have shown that PKD promotes invasion (Ochi et al., 2011), others have reported that it opposes invasive migration and is downregulated in aggressive metastatic disease (Eiseler et al., 2009; Kim et al., 2008; Zhang et al., 2007). Indeed, we have previously demonstrated that suppression of PKD can promote α5β1-integrin dependent invasion of gastric cancer cells (Kim et al., 2008). The present study supports a role for PKD-mediated phosphorylation of Rabaptin-5 in cancer cell invasion, but crucially provides mechanistic insight into how this depends on the nature of the surrounding ECM. By promoting αvβ3 recycling, Rabaptin-5 phosphorylation negatively impacts invasion into fibronectin-rich matrices. Thus, under these circumstances, reduction of invasion by PKD-Rabaptin-5 signaling is specifically due to the inhibition exerted by short-loop αvβ3 recycling over that of α5β1 (Figure 6). However, in microenvironments that are fibronectin-deficient, where invasion is dependent on αvβ3 and not α5β1, Rabaptin-5 phosphorylation is a strong driver of tumor cell invasion. Moreover, our data indicate that PKD-Rabaptin-5 signaling influences α5β1-dependent invasion by intersecting with pathways that are also influenced by mutant p53. In view of this it will be interesting to determine the relationship between Rabaptin-5 phosphorylation and mutant p53 status in aggressive metastatic cancer.

These findings not only provide mechanistic insights into the control of cell motility but also provide evidence for a signal relay pathway that modulates endocytic and recycling transport steps. Whether the PKD-Rabaptin-5 signaling network impacts pathophysiological conditions in which integrin recycling and cell migration are key phenotypes remains to be determined, but what is clear from these findings is that the relative contribution made by αvβ3 and α5β1 integrins to the invasion and metastasis of tumors following the silencing of PKD expression should be considered, as inhibitors that target this kinase approach the clinic.

Experimental Procedures

Antibodies, Immunoblotting and Immunoprecipitation

Following 24 hr serum starvation, cells were lysed in RIPA lysis buffer (150 mM Tris/HCl, pH 7.5, 150 mM NaCl, 1% NP-40, 0.5% SDC, 0.1% SDS, 50 nM calyculin, 1 mM PMSF) plus protease inhibitor cocktail (Sigma-Aldrich). For immunoprecipitation, cells were incubated for 2 hr with 1 μg anti-Myc or anti-Rabaptin-5 followed by a 2 hr incubation with protein G-Agarose (Amersham Biosciences). Immune complexes were washed three times with NETN (20 mM Tris/HCl, pH 8.0, 100 mM NaCl, 0.5% NP-40, 1 mM EDTA, pH 8.0) and resolved by SDS-PAGE or subjected to kinase assays.

For immunoprecipitations to determine the association between Rabaptin-5 and Rab4 and Rab5, cells were trypsinized and then allowed to adhere to culture plates that had been

previously coated with bovine fibronectin (Sigma) for 2 hr. PDGF-BB (10 ng/ml) was added to the cells for 1 hr prior to lysis in a buffer containing 200 mM NaCl, 75 mM Tris-HCl, pH 7, 15 mM NaF, 1.5 mM Na_3VO_4, 7.5 mM EDTA, 7.5 mM EGTA, 0.15% (vol/vol) Tween-20, 50 μg/ml leupeptin, 50 μg/ml aprotinin, and 1 mM 4-(2-aminoethyl)-benzenesulfonyl fluoride). Lysates were passed three times through a 25-gauge needle and clarified by centrifugation at 10,000 g for 10 min at 4 °C. Magnetic beads conjugated to sheep anti-mouse IgG (Invitrogen) were bound to anti-myc (9B11, Cell Signaling Technologies) antibody. Antibody-coated beads were incubated with lysates for 2 h at 4 °C with constan t rotation. Unbound proteins were removed by two 2 min washes in lysis buffer, and the presence of myc-Rabaptin-5 and Cherry-Rab GTPases was determined by immunoblotting with anti-myc, anti-Rabaptin-5 or an antibody raised against dsRed which recognizes mCherry.

The anti-PKD (C-20), anti-c-Myc (9E10), and anti-Rabaptin-5 (H300) antibodies were from Santa Cruz Biotechnology (Santa Cruz, CA); anti-PKD pS916 and pS744/748 antibodies were from Cell Signaling Technology (Danvers, MA); anti-HA was purified in-house from the 12CA5 hybridoma. The p85 antibody was described previously (Kapeller et al., 1995). Anti-β-actin was from Sigma (Sigma-Pierce). The anti-PKD pMOTIF antibody has been described (Doppler et al., 2005). Anti-dsRed that recognizes mCherry was from Clontech. Mouse anti-hβ3 (#555752), hamster anti-mβ3 (#01861D), mouse anti-hα5 (#555651), and rat anti-mα5 (#553319) were from BDPharmingen (NJ, USA).

Cell Culture

HEK293T, NIH-3T3 and MDA-MD-231 cells were maintained in high glucose Dulbecco's modified Eagle's medium supplemented with 10% fetal bovine serum. LnCap and A2780 cells were maintained in RPMI 1640 medium supplemented with 10% fetal bovine serum. HEK293T cells were transiently transfected with polyethylenimine (PEI) gene transfer reagent (Boussif et al., 1995) in its 25-kDa linear form (Polysciences, Warrington, PA) and all other cells were transiently transfected with Lipofectamine 2000 (Invitrogen, Carlsbad, CA). Briefly, 6 μg of DNA was mixed with 18 μg of linear 25-kDa PEI or 7 μg DNA was mixed with 18 μg Lipofectamine in a total volume of 400 μl of GIBCO reduced serum OPTI-MEM medium (GIBCO, Rockford, MD). After 25 min incubation, the mixture was combined with HEK293T cells in suspension or on sub-confluent plates of NIH3T3, LnCap, or HeLa cells. Cells were treated with PDBu (Sigma), PMA (Alexis Biochem), and PDGF (R&D Systems) and EGF (R&D Systems) at the indicated concentrations for 30 min or indicated times after overnight serum-starvation. Gö6976 (Calbiochem) was used at 1 μM and MG-132 (Calbiochem) was used at 10 μM. Transfection of all vectors, shRNA and siRNA oligonucleotides (Dharmacon) into NIH3T3, A2780 and MDA-MB-231 cells was carried out using the Amaxa 'Nucleofector' system according to manufacturer's instructions. Solution T, program A-23 was used for A2780 and solution V, program X-13 for MDA-MB-231 cells, and solution R, program T-20 was used for NIH3T3 cells.

Lentiviral infection

pLKO.1 plasmid constructs were co-transfected in HEK293T cells with packaging vectors pCMV-Δ8.2 and pCMV-VSVG using polyethyleimine. Two days post-transfection, virus-containing media was harvested, 5 μg of Polybrene added, passed through a 0.45 μM filter, and used to infect target cells. Target cells at approximately 70% confluence were infected for 24 hr followed by selection in 2 μg/mL puromycin for 48 hr prior to stimulation and cell lysis.

In Vitro Kinase Assay

Rabaptin-5 constructs were expressed in HEK293T cells and immunoprecipitated with Myc antibody. Immune complexes were incubated with recombinant human GST-PKD1 and kinase buffer from Cell Signaling Technology (Danvers, MA) in the presence of 200 μM cold ATP and 5 μCurie γ^{32}P[ATP] for 40 min at 30°C. Samples were resolved by SDS-PAGE and phosphorylation was detected using autoradiography.

Integrin recycling assay

Following surface labeling at 4°C with 0.2 mg/ml NHS-SS-biotin, cells were transferred to serum-free DMEM at 22°C for 15 min or 30 min at 37°C to allow internalization of tracer into early endosomes and the perinuclear recycling compartment, respectively. Cells were returned to ice and washed twice with ice-cold PBS, and biotin was removed from proteins remaining at the cell surface by reduction with MesNa Sodium 2-sulfanylethanesulfonate (Sigma). The internalized fraction was then chased from the cells by returning them to 37°C in serum-free DMEM in the absence or presence of 10 ng/ml PDGF. At the indicated times, cells were returned to ice and biotin was removed from recycled proteins by a second reduction with MesNa. Intracellular biotinylated integrins were then determined by capture-ELISA.

Capture-ELISA

Maxisorb 96-well plates (Life Technologies) were coated overnight with 5 μg/ml appropriate anti-integrin antibodies in 0.05 M Na_2CO_3 (pH 9.6) at 4°C and were blocked in PBS containing 0.05% Tween-20 (PBS-T) with 5% BSA for 1 hr at room temperature. Integrins were captured by overnight incubation of 50 μl cell lysate at 4°C. Unbound material was removed by extensive washing with PBS-T, and wells were incubated with streptavidin-conjugated horseradish peroxidase (Amersham) in PBS-T containing 1% BSA for 1 hr at 4°C. Following further washing, biotinylated integrins were detected by a chromogenic reaction with ortho-phenylenediamine.

Time-lapse microscopy and track-plot analysis

Confluent monolayers were wounded with a plastic pipette tip and placed on the stage of an inverted microscope (Axiovert S100; Carl Zeiss Micro-Imaging, Inc.) in an atmosphere of 5% CO2 at 37°C. Cells were observed using a 10x phase-contrast objective, and images were collected every 10 min using a digital camera (C47 42–95; Hamamatsu). Videos were generated and cell tracks analyzed using ImageJ software. Cell-derived matrix (CDM) was generated as described previously (Bass et al., 2007; Cukierman et al., 2001), but with telomerase immortalized fibroblasts being substituted for primary cultured human dermal fibroblasts without any noticeable alteration to the results. A2780 cells were plated onto CDM 4 hr prior to imaging by time-lapse phase contrast microscopy as described above.

Cell imaging

NIH3T3 cells were seeded onto glass-bottom 3 cm plates grown to confluence and wounded with a plastic pipette tip. Cells migrating into the wounds were imaged with a 64x objective of an inverted confocal microscope (Fluoview FV1000, Olympus) in an atmosphere of 5% CO_2 at 37°C. To quantify co-localization we used a macro to operate within the Image J program that applies the algorithm developed by Jaskolsky et al (Jaskolski et al., 2005). This automated method is based on edge detection and calculation of signal intensity deviation and leads to the generation of a pseudocolour image of the correlated signals from the green and red images. The number of red pixels (Cherry-Rab4) co-localizing with the green (GFP-Rabaptin-5) was then expressed as a percentage of the total quantity of red pixels.

Inverted invasion assay

Inverse invasion assays were performed as described previously (Hennigan et al., 1994). Briefly, complete Matrigel was diluted in an equal volume of ice-cold PBS with or without addition of soluble fibronectin (25 μg/ml final concentration). 100 μl of the diluted Matrigel mix was pipetted into a Transwell (8 μm diameter pores), inserted into a well of a 24-well tissue culture plate, and left to set at 37°C. Transwells were then inverted and 4×10^4 cells were placed on the underside of the filter. Transwells were then covered with the base of the 24-well tissue culture plate so that they made contact with cell suspension droplets. Cell attachment was allowed to proceed for 4 hr, before the plate was inverted back and the non-adherent cells were washed off by three sequential washes in 1 ml serum-free medium. Transwells were placed in 1 ml of serum-free medium, which constituted the lower chamber of the assay, and 100 μl of 10% FCS-RPMI supplemented with 25 ng/ml EGF was pipetted on top of the Transwell. The cells were then allowed to invade into the Matrigel and towards the gradient of serum and EGF for 48 hr at 37°C in the atmosphere of 5% CO_2. To visualise cells that migrated into the Matrigel plug, 4 μM Calcein AM (acetoxymethyl ester of calcein) was used. After 1 hr at 37°C the cells were imaged by confocal microscopy using a Leica SP2 confocal microscope and a 20x objective at an excitation wavelength of 488 nm and emission wavelength of 515nm. Optical sections were captured at 10 μm or 15 μm intervals, starting from the underside of the Transwell filter and moving upwards in the direction of cell invasion. The resulting images were quantified and assembled into invasive strips using Image J software. The threshold fluorescence intensity of the images was set to only register cells that lay within each individual optical slice, and the sum of the fluorescence in the sections from 40 μm or 45 μm and above was divided by the total fluorescence of all the sections. Data were generated from at least 3 individual experiments, in which each condition was represented by three Transwells and optical sections were taken from at least 3 areas of each Transwell.

Supplementary Material

Refer to Web version on PubMed Central for supplementary material.

Acknowledgments

We thank Juan Bonifacino and Peter Storz for providing reagents, and Lewis Cantley, Sheila Thomas, Jeffrey Settleman, Patricia Muller, Karen Vousden and members of the Toker, Norman and Wenyi Wei laboratories for advice and discussions. This study was supported in part by grants from the National Institutes of Health (A.T., CA075134 and CA096710), The Department of Defense Breast Cancer Research program (C.C., BC061404), Cancer Research UK (J.C.N. and E.R.) and the Genesis Oncology Trust of New Zealand (K.K.B, GOT-1040-JGPDF). E.R. is supported by a fellowship from the West of Scotland Women's Bowling Association.

Bibliography

Bass MD, Roach KA, Morgan MR, Mostafavi-Pour Z, Schoen T, Muramatsu T, Mayer U, Ballestrem C, Spatz JP, Humphries MJ. Syndecan-4-dependent Rac1 regulation determines directional migration in response to the extracellular matrix. The Journal of cell biology. 2007; 177:527–538. [PubMed: 17485492]

Boussif O, Lezoualc'h F, Zanta MA, Mergny MD, Scherman D, Demeneix B, Behr JP. A versatile vector for gene and oligonucleotide transfer into cells in culture and in vivo: polyethylenimine. Proc Natl Acad Sci U S A. 1995; 92:7297–7301. [PubMed: 7638184]

Caswell PT, Chan M, Lindsay AJ, McCaffrey MW, Boettiger D, Norman JC. Rab-coupling protein coordinates recycling of alpha5beta1 integrin and EGFR1 to promote cell migration in 3D microenvironments. J Cell Biol. 2008; 183:143–155. [PubMed: 18838556]

Caswell PT, Spence HJ, Parsons M, White DP, Clark K, Cheng KW, Mills GB, Humphries MJ, Messent AJ, Anderson KI, et al. Rab25 associates with alpha5beta1 integrin to promote invasive migration in 3D microenvironments. Dev Cell. 2007; 13:496–510. [PubMed: 17925226]

Caswell PT, Vadrevu S, Norman JC. Integrins: masters and slaves of endocytic transport. Nat Rev Mol Cell Biol. 2009; 10:843–853. [PubMed: 19904298]

Cukierman E, Pankov R, Stevens DR, Yamada KM. Taking cell-matrix adhesions to the third dimension. Science. 2001; 294:1708–1712. [PubMed: 11721053]

Deneka M, Neeft M, Popa I, van Oort M, Sprong H, Oorschot V, Klumperman J, Schu P, van der Sluijs P. Rabaptin-5alpha/rabaptin-4 serves as a linker between rab4 and gamma(1)-adaptin in membrane recycling from endosomes. EMBO J. 2003; 22:2645–2657. [PubMed: 12773381]

Dephoure N, Zhou C, Villen J, Beausoleil SA, Bakalarski CE, Elledge SJ, Gygi SP. A quantitative atlas of mitotic phosphorylation. Proc Natl Acad Sci U S A. 2008; 105:10762–10767. [PubMed: 18669648]

di Blasio L, Droetto S, Norman J, Bussolino F, Primo L. Protein kinase D1 regulates VEGF-A-induced alphavbeta3 integrin trafficking and endothelial cell migration. Traffic. 2010; 11:1107–1118. [PubMed: 20477989]

Doppler H, Storz P, Li J, Comb MJ, Toker A. A phosphorylation state-specific antibody recognizes Hsp27, a novel substrate of protein kinase D. The Journal of biological chemistry. 2005; 280:15013–15019. [PubMed: 15728188]

Eiseler T, Doppler H, Yan IK, Goodison S, Storz P. Protein kinase D1 regulates matrix metalloproteinase expression and inhibits breast cancer cell invasion. Breast Cancer Res. 2009; 11:R13. [PubMed: 19243594]

Fan GH, Lapierre LA, Goldenring JR, Sai J, Richmond A. Rab11-family interacting protein 2 and myosin Vb are required for CXCR2 recycling and receptor-mediated chemotaxis. Mol Biol Cell. 2004; 15:2456–2469. [PubMed: 15004234]

Fugmann T, Hausser A, Schoffler P, Schmid S, Pfizenmaier K, Olayioye MA. Regulation of secretory transport by protein kinase D-mediated phosphorylation of the ceramide transfer protein. J Cell Biol. 2007; 178:15–22. [PubMed: 17591919]

Gu Z, Noss EH, Hsu VW, Brenner MB. Integrins traffic rapidly via circular dorsal ruffles and macropinocytosis during stimulated cell migration. The Journal of cell biology. 2011; 193:61–70. [PubMed: 21464228]

Hausser A, Storz P, Martens S, Link G, Toker A, Pfizenmaier K. Protein kinase D regulates vesicular transport by phosphorylating and activating phosphatidylinositol-4 kinase IIIbeta at the Golgi complex. Nature cell biology. 2005; 7:880–886.

Hennigan RF, Hawker KL, Ozanne BW. Fos-transformation activates genes associated with invasion. Oncogene. 1994; 9:3591–3600. [PubMed: 7970719]

Jackson TR, Brown FD, Nie Z, Miura K, Foroni L, Sun J, Hsu VW, Donaldson JG, Randazzo PA. ACAPs are arf6 GTPase-activating proteins that function in the cell periphery. J Cell Biol. 2000; 151:627–638. [PubMed: 11062263]

Jaskolski F, Mulle C, Manzoni OJ. An automated method to quantify and visualize colocalized fluorescent signals. J Neurosci Methods. 2005; 146:42–49. [PubMed: 15935219]

Jones MC, Caswell PT, Norman JC. Endocytic recycling pathways: emerging regulators of cell migration. Current opinion in cell biology. 2006; 18:549–557. [PubMed: 16904305]

Kapeller R, Toker A, Cantley LC, Carpenter CL. Phosphoinositide 3-kinase binds constitutively to alpha/beta-tubulin and binds to gamma-tubulin in response to insulin. J Biol Chem. 1995; 270:25985–25991. [PubMed: 7592789]

Kim M, Jang HR, Kim JH, Noh SM, Song KS, Cho JS, Jeong HY, Norman JC, Caswell PT, Kang GH, et al. Epigenetic inactivation of protein kinase D1 in gastric cancer and its role in gastric cancer cell migration and invasion. Carcinogenesis. 2008; 29:629–637. [PubMed: 18283041]

Li J, Ballif BA, Powelka AM, Dai J, Gygi SP, Hsu VW. Phosphorylation of ACAP1 by Akt regulates the stimulation-dependent recycling of integrin beta1 to control cell migration. Dev Cell. 2005; 9:663–673. [PubMed: 16256741]

Mai A, Veltel S, Pellinen T, Padzik A, Coffey E, Marjomaki V, Ivaska J. Competitive binding of Rab21 and p120RasGAP to integrins regulates receptor traffic and migration. The Journal of cell biology. 2011; 194:291–306. [PubMed: 21768288]

Muller PA, Caswell PT, Doyle B, Iwanicki MP, Tan EH, Karim S, Lukashchuk N, Gillespie DA, Ludwig RL, Gosselin P, et al. Mutant p53 drives invasion by promoting integrin recycling. Cell. 2009; 139:1327–1341. [PubMed: 20064378]

Nhek S, Ngo M, Yang X, Ng MM, Field SJ, Asara JM, Ridgway ND, Toker A. Regulation of oxysterol-binding protein Golgi localization through protein kinase D-mediated phosphorylation. Molecular biology of the cell. 2010:2327–2337. [PubMed: 20444975]

Ochi N, Tanasanvimon S, Matsuo Y, Tong Z, Sung B, Aggarwal BB, Sinnett-Smith J, Rozengurt E, Guha S. Protein kinase D1 promotes anchorage-independent growth, invasion, and angiogenesis by human pancreatic cancer cells. J Cell Physiol. 2011; 226:1074–1085. [PubMed: 20857418]

Pellinen T, Arjonen A, Vuoriluoto K, Kallio K, Fransen JA, Ivaska J. Small GTPase Rab21 regulates cell adhesion and controls endosomal traffic of beta1-integrins. The Journal of cell biology. 2006; 173:767–780. [PubMed: 16754960]

Pellinen T, Ivaska J. Integrin traffic. Journal of cell science. 2006; 119:3723–3731. [PubMed: 16959902]

Powelka AM, Sun J, Li J, Gao M, Shaw LM, Sonnenberg A, Hsu VW. Stimulation-dependent recycling of integrin beta1 regulated by ARF6 and Rab11. Traffic. 2004; 5:20–36. [PubMed: 14675422]

Rainero E, Caswell PT, Muller PA, Grindlay J, McCaffrey MW, Zhang Q, Wakelam MJ, Vousden KH, Graziani A, Norman JC. Diacylglycerol kinase alpha controls RCP-dependent integrin trafficking to promote invasive migration. J Cell Biol. 2012; 196:277–295. [PubMed: 22270919]

Ramsay AG, Marshall JF, Hart IR. Integrin trafficking and its role in cancer metastasis. Cancer Metastasis Rev. 2007; 26:567–578. [PubMed: 17786537]

Roberts M, Barry S, Woods A, van der Sluijs P, Norman J. PDGF-regulated rab4-dependent recycling of alphavbeta3 integrin from early endosomes is necessary for cell adhesion and spreading. Curr Biol. 2001; 11:1392–1402. [PubMed: 11566097]

Rykx A, De Kimpe L, Mikhalap S, Vantus T, Seufferlein T, Vandenheede JR, Van Lint J. Protein kinase D: a family affair. FEBS Lett. 2003:81–86. [PubMed: 12829240]

Shattil SJ, Kim C, Ginsberg MH. The final steps of integrin activation: the end game. Nat Rev Mol Cell Biol. 2010; 11:288–300. [PubMed: 20308986]

Skalski M, Coppolino MG. SNARE-mediated trafficking of alpha5beta1 integrin is required for spreading in CHO cells. Biochem Biophys Res Commun. 2005; 335:1199–1210. [PubMed: 16112083]

Stenmark H, Vitale G, Ullrich O, Zerial M. Rabaptin-5 is a direct effector of the small GTPase Rab5 in endocytic membrane fusion. Cell. 1995; 83:423–432. [PubMed: 8521472]

van der Sluijs P, Mohrmann K, Deneka M, Jongeneelen M. Expression and properties of Rab4 and its effector rabaptin-4 in endocytic recycling. Methods Enzymol. 2001; 329:111–119. [PubMed: 11210527]

Vega RB, Harrison BC, Meadows E, Roberts CR, Papst PJ, Olson EN, McKinsey TA. Protein kinases C and D mediate agonist-dependent cardiac hypertrophy through nuclear export of histone deacetylase 5. Molecular and cellular biology. 2004; 24:8374–8385. [PubMed: 15367659]

Villen J, Beausoleil SA, Gerber SA, Gygi SP. Large-scale phosphorylation analysis of mouse liver. Proceedings of the National Academy of Sciences of the United States of America. 2007; 104:1488–1493. [PubMed: 17242355]

Vitale G, Rybin V, Christoforidis S, Thornqvist P, McCaffrey M, Stenmark H, Zerial M. Distinct Rab-binding domains mediate the interaction of Rabaptin-5 with GTP-bound Rab4 and Rab5. Embo J. 1998; 17:1941–1951. [PubMed: 9524117]

Vukmirica J, Monzo P, Le Marchand-Brustel Y, Cormont M. The Rab4A effector protein Rabip4 is involved in migration of NIH 3T3 fibroblasts. J Biol Chem. 2006; 281:36360–36368. [PubMed: 17001082]

White DP, Caswell PT, Norman JC. alpha v beta3 and alpha5beta1 integrin recycling pathways dictate downstream Rho kinase signaling to regulate persistent cell migration. The Journal of cell biology. 2007; 177:515–525. [PubMed: 17485491]

Woods AJ, White DP, Caswell PT, Norman JC. PKD1/PKCmu promotes alphavbeta3 integrin recycling and delivery to nascent focal adhesions. The EMBO journal. 2004; 23:2531–2543. [PubMed: 15192707]

Yoon SO, Shin S, Mercurio AM. Hypoxia stimulates carcinoma invasion by stabilizing microtubules and promoting the Rab11 trafficking of the alpha6beta4 integrin. Cancer Res. 2005; 65:2761–2769. [PubMed: 15805276]

Zhang K, Ye C, Zhou Q, Zheng R, Lv X, Chen Y, Hu Z, Guo H, Zhang Z, Wang Y, et al. PKD1 inhibits cancer cells migration and invasion via Wnt signaling pathway in vitro. Cell Biochem Funct. 2007; 25:767–774. [PubMed: 17437318]

Zugaza JL, Sinnett-Smith J, Van Lint J, Rozengurt E. Protein kinase D (PKD) activation in intact cells through a protein kinase C-dependent signal transduction pathway. The EMBO journal. 1996; 15:6220–6230. [PubMed: 8947045]

Highlights

- Rabaptin-5, a Rab5 effector in endosomal fusion, is a protein kinase D substrate
- Rabaptin-5 phosphorylation controls αvβ3 integrin recycling from early endosomes
- Rabaptin-5 phosphorylation promotes cell migration and αvβ3-dependent invasion
- Rabaptin-5 phosphorylation opposes α5β1-dependent recycling and invasion

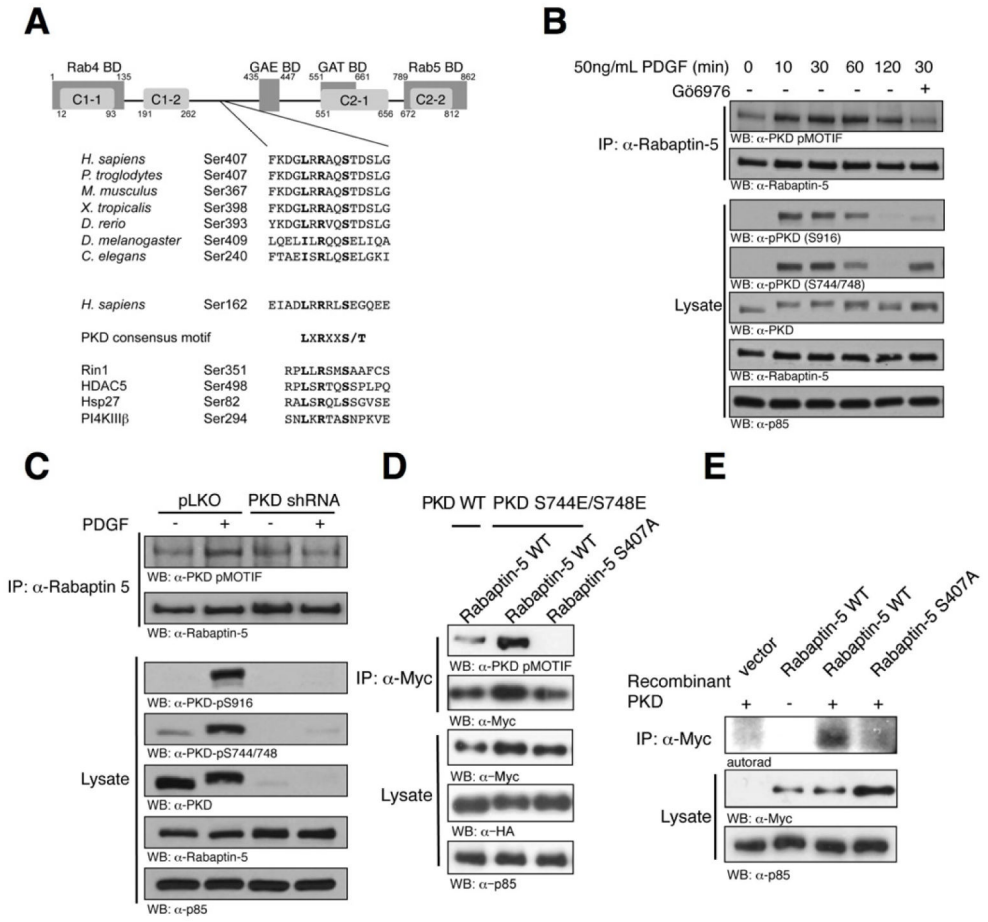

Figure 1. PKD phosphorylates Rabaptin-5

(A) Schematic of Rabaptin-5 showing domain structure and PKD consensus phosphorylation motifs and Ser407 and Ser162. The Ser407 motif is evolutionarily conserved. Also shown is the optimal PKD consensus phosphorylation motif, and the phosphorylation sites in the PKD substrates Rin1, HDAC5, Hsp27 and PI4KIIIβ. Rabaptin-5 contains four coiled-coil motifs (C1-1, C1-2, C2-1, C2-2), an amino-terminal Rab4 binding domain, a carboxyl-terminal Rab5 binding domain, and two Golgi-localized Gamma ear-containing Arf-binding protein (GGA) binding sites (GAE BD and GAT BD).

(B) NIH-3T3 cells were serum starved for 20 hr and then stimulated with 50 ng/ml PDGF. Where indicated, cells were pretreated with PKC/PKD inhibitor, Gö6976 (1 μM). Endogenous Rabaptin-5 was immunoprecipitated with anti-Rabaptin-5 and immunoblotted with the anti-PKD pMOTIF antibody. In all panels, total cell lysates were also immunoblotted with the indicated antibodies (p85 served as loading control). All results are representative of at least three independent experiments.

(C) NIH-3T3 cells were transfected with either pLKO vector or PKD1 plus PKD2 shRNA. After selection cells were serum-starved and stimulated with 50 ng/ml PDGF or DMSO for 30 min. Rabaptin-5 immunoprecipitates were immunoblotted with the anti-PKD pMOTIF antibody.

(D) HEK293T cells were co-transfected with Myc-Rabaptin-5 WT or Myc-Rabaptin-5 Ser407Ala, and either PKD WT or PKD S744E/S748E, as indicated and serum-starved overnight. Rabaptin-5 immunoprecipitates were immunoblotted with anti-PKD pMOTIF antibody.

(E) LnCap cells transfected with Myc-Rabaptin-5 WT or Myc-Rabaptin-5 Ser407Ala were serum-starved, and Rabaptin-5 immunoprecipitated with anti-Myc. Immune complexes were then incubated in kinase assay buffer containing γ^{32}P-[ATP] in the absence or presence of purified recombinant PKD1. Rabaptin-5 phosphorylation was detected by autoradiography. Total cell lysates were immunoblotted with the indicated antibodies. All results are representative of at least three independent experiments.

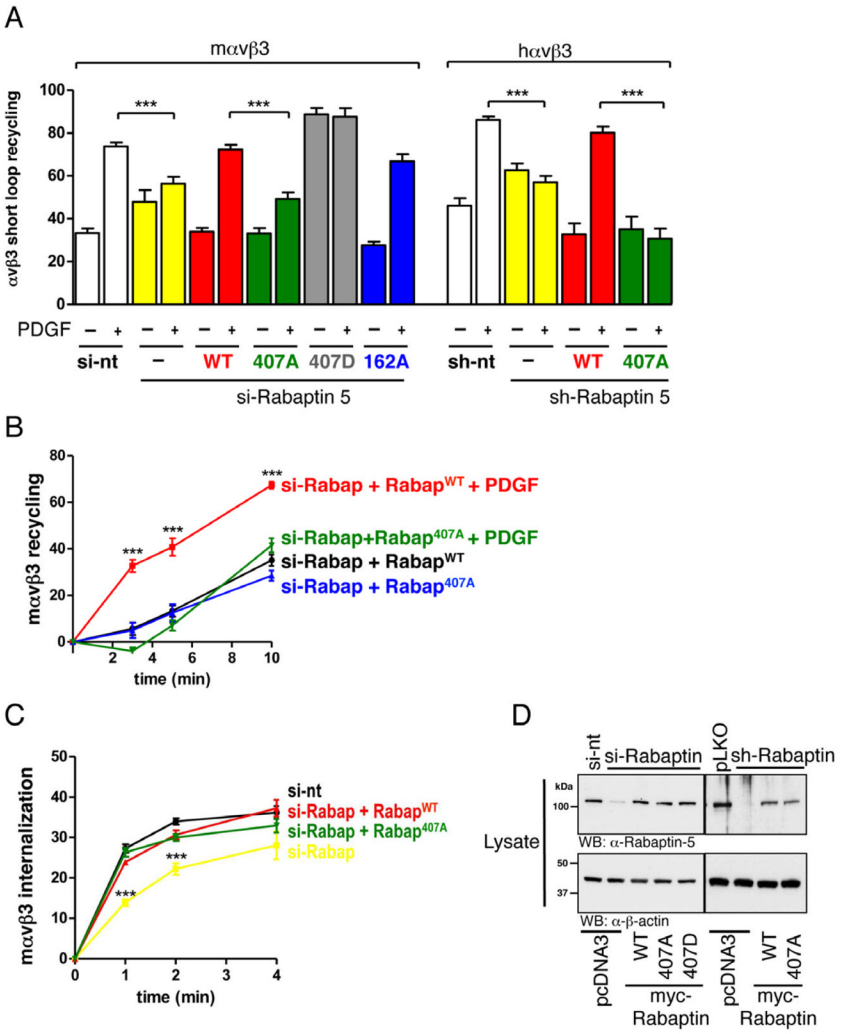

Figure 2. Rabaptin-5 phosphorylation is required for PDGF-driven αvβ3 integrin recycling

(A–B) NIH 3T3 fibroblasts were transfected with either non-targeting siRNA (si-nt), Rabaptin-5 siRNA (si-Rabaptin-5), or infected with Rabaptin-5 shRNA (sh-Rabaptin-5). Cells were also co-transfected with si- or sh-RNA resistant Rabaptin-5 mutants (vector control, yellow bars; WT, red bars; Ser407Ala, green bars; Ser407Asp, grey bars; Ser162Ala, blue bars). After selection, cells were transfected with human (hαvβ3) αvβ3 integrin where indicated. Cells were surface labeled with 0.2 mg/ml NHS-SS-biotin for 30 min at 4°C, and internalization was allowed to proceed for 15 min at 22°C. Cells were exposed to MesNa at 4°C to remove surface biotin, and internalized integrin was chased back to the cell surface at 37°C for 10 min (A), or for the indicated times (B) in the absence and presence of 10 ng/ml PDGF. Cells were then re-exposed to MesNa, and levels of intracellular biotinylated integrin were determined by capture-ELISA using microtiter wells coated with anti-human β3 monoclonal or anti-mouse β3 antibodies. Values are mean ±SEM. ***P<0.0001; **P<0.0022 (Mann-Whitney test).

(C) NIH 3T3 fibroblasts transfected as in (A) were surface labeled with 0.2 mg/ml NHS-SS-biotin for 30 min at 4°C and then plac ed at 37°C for indicated times in the presence of 0.6 mM primaquine to inhibit receptor recycling. Biotin was removed by MesNa treatment at 4°C, cells lysed and biotinylated integrin determined by capture-ELISA as for (A). All

results are representative of at least three independent experiments. Values are mean ±SEM. ***P<0.001 (Mann-Whitney test).

(D) Immunoblot analysis from the experiments in (A–C). Cell lysates obtained from each condition were immunoblotted with anti-Rabaptin-5 or anti-β-actin control.

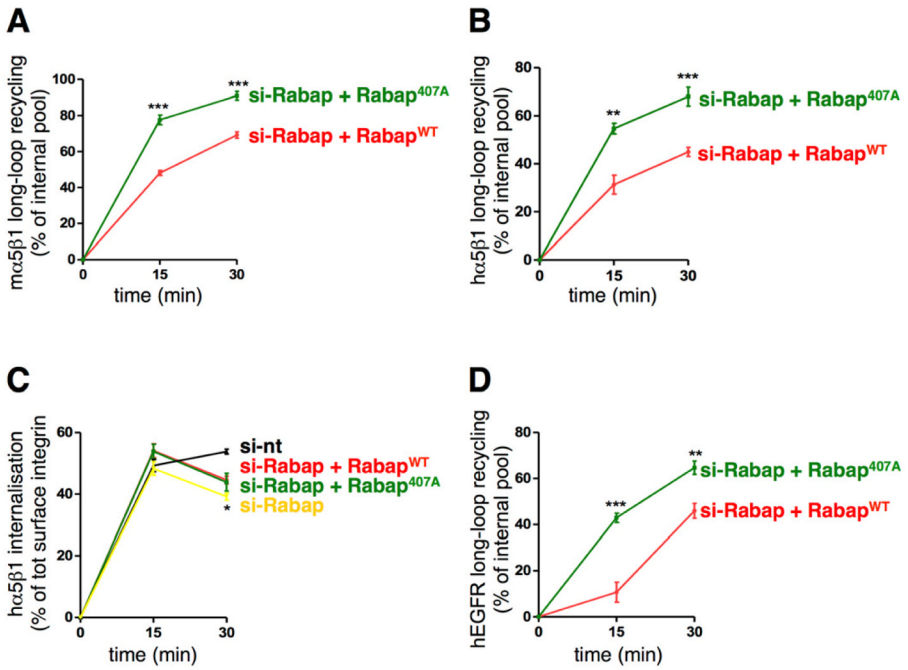

Figure 3. Rabaptin-5 phosphorylation negatively regulates α5β1 integrin and EGFR recycling

NIH 3T3 fibroblasts (A, C) and A2780 cells (B, D) were co-transfected with Rabaptin-5 siRNA (si-Rabaptin-5) and Rabaptin-5 siRNA-resistant mutants (WT, Ser407A). Integrin recycling (A, B) and internalization (C) was determined as in Figure 2, but with the internalization time increased to 30 min to measure long-loop recycling and the ELISA plate coated with anti-α5 monoclonal antibodies. In (D), recycling was determined as for (B), but with the ELISA plate coated with antibodies recognizing EGFR. All results are representative of at least three independent experiments. Values are mean ±SEM. ***P<0.001; **P<0.005 *P<0.0286 (Mann-Whitney test).

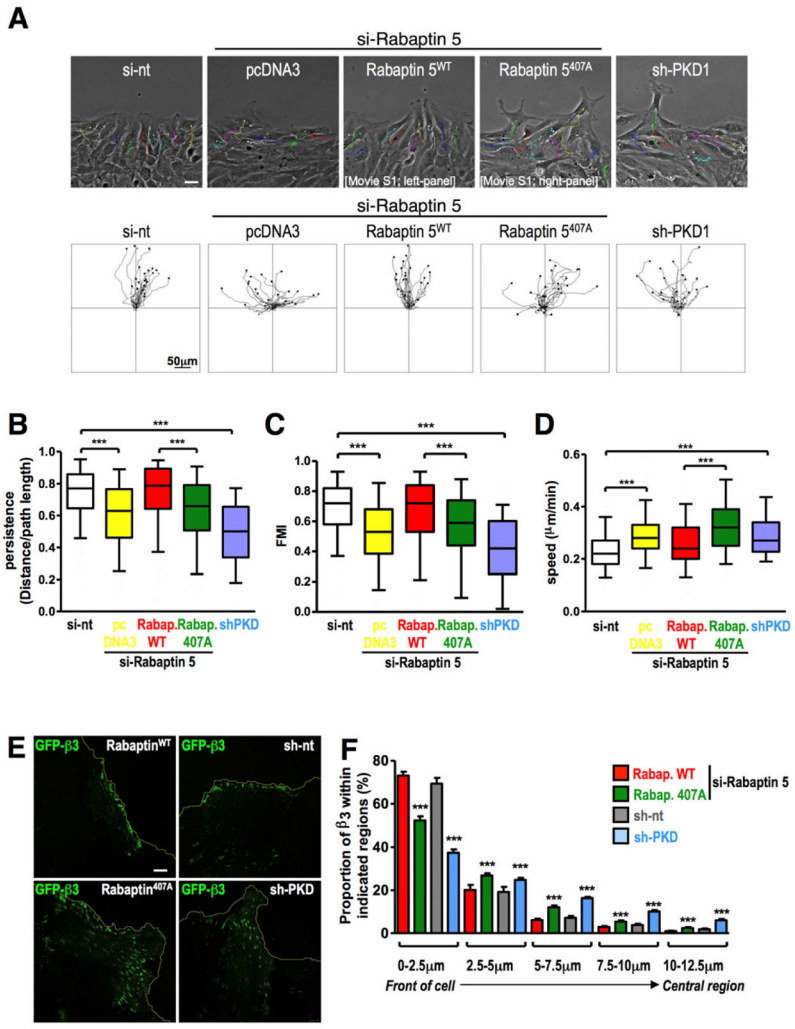

Figure 4. Rabaptin-5 phosphorylation regulates delivery of αvβ3 to the leading edge and migratory persistence on 2D surfaces

(A) Confluent monolayers of NIH 3T3 fibroblasts were transfected with PKD shRNA (sh-PKD) or Rabaptin-5 siRNA (si-Rabaptin-5) or non-targeting siRNA (si-nt), and co-transfected with vector control (−) or Rabaptin-5 siRNA-resistant mutants (WT, Ser407Ala). Monolayers were wounded and cells allowed to migrate into the wound. Cells were tracked by time-lapse video microscopy, with frames captured at 10 min intervals. The position of the cell nucleus was followed using cell tracking software, and cumulative track plots of individual cells are highlighted (bar, 50 μm).

(B–D) The speed (B), persistence (C) and forward migration index (FMI) (D) of cell migration obtained from the conditions in (A) were extracted from the track plots. Persistence is defined as the ratio of the vectorial distance traveled to the total path length described by the cell. See also movies S1A and S1B from which Figures 5A (si-Rabaptin 5 + RabWT and si-Rabaptin-5 + Rab407Ala, respectively) are taken. All results are representative of at least three independent experiments. *** = $p<0.0001$ (Mann-Whitney test). The box-and-whiskers plots represent: median line; box=quartiles; whiskers=5–95% confidence.

(E, F) NIH 3T3 fibroblasts were transfected with PKD shRNA (sh-PKD), Rabaptin-5 siRNA or non-targeting siRNA (si-nt), and co-transfected with vector control (−) or Rabaptin-5

siRNA-resistant mutants (WT, Ser407Ala). All cells were then transfected with GFP-β3 integrin and grown to confluence. Monolayers were wounded and images captured of the cells migrating into the wound. The fluorescence images in (E) are representative frames from these movies, and the wound's edge is denoted by the yellow line (bar, 10 μm). The distribution of αvβ3 was determined by using a macro that describes regions running progressively from the cell edge to the cell center, and determining the proportion of GFP-β3 that was present at the indicated distances from the cell edge (F). Values are mean ±SEM from three independent experiments, *** = $p<0.0001$ (Mann-Whitney test).

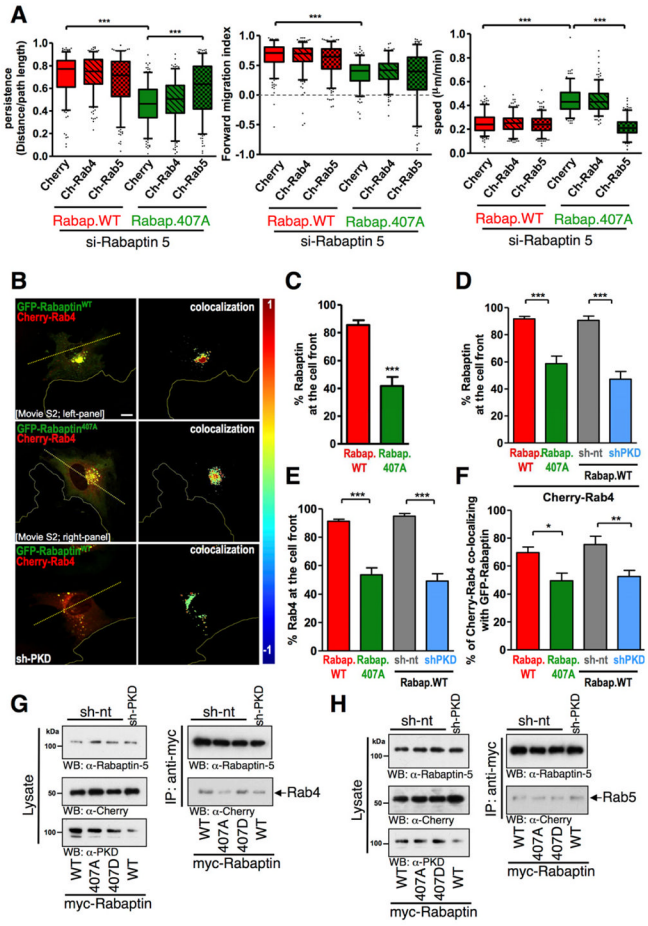

Figure 5. Rabaptin-5 phosphorylation regulates its association with Rab4 at the front of migrating cells

(A) NIH 3T3 fibroblasts were transfected with Rabaptin-5 siRNA (si-Rabaptin-5) in combination with Rabaptin-5 siRNA-resistant mutants (WT, Ser407Ala) and either Cherry alone, Cherry-tagged Rab4 (Ch-Rab4) or Cherry-tagged Rab5 (Ch-Rab5). The speed, persistence and forward migration index of cells migrating into scratch-wounds was determined as for Figure 4B–D. ***P<0.0001 (Mann-Whitney test). The box-and-whiskers plots represent: median line; box=quartiles; whiskers=5–95% confidence.

(B–F) NIH 3T3 fibroblasts were transfected with Rabaptin-5 siRNA and Cherry-Rab4 in combination with si-RNA resistant GFP-Rabaptin-5 or GFP-Rabaptin Ser407Ala as indicated. Where indicated the cells were co-transfected with a short-hairpin targeting PKD1 (sh-PKD) or a non-targeting control (sh-nt). Cells were allowed to migrate into scratch-wounds for 2–4 hr and the distribution of GFP-Rabaptin-5 (green) and Cherry-Rab4 (red) was imaged by live cell confocal microscopy (B; yellow line indicates the wound edge). The proportion of cellular GFP-Rabaptin-5 and Cherry-Rab4 fluorescence that was present anterior to a line drawn through the center of the nucleus and parallel to the wound edge (dotted yellow line) was determined using Image J as described in the methods (C–F). The pixel by pixel co-localization of the GFP-Rabaptin-5 with Cherry-Rab4 was determined using an algorithm as described in the methods section (Jaskolski et al., 2005); areas of high co-localization are depicted by the red pseudocolour, and pixels in which the GFP-Rabaptin-5 or Cherry-Rab4 were present but not co-localized with one another are represented by the blue pseudocolour (B). Values extracted from these analyses are the

mean ±SEM of three independent experiments (F). ***P<0.0001; **P<0.0059; *P<0.0174 (Mann-Whitney test).

(G-H) NIH 3T3 fibroblasts were transfected with myc-Rabaptin-5 or the indicated myc-tagged Rabaptin-5 mutants in combination with Cherry-Rab4 (G) or Cherry-Rab5 (H). Where indicated the cells were co-transfected with a short-hairpin targeting PKD1 (sh-PKD) or a non-targeting control (sh-nt). Transfected cells were trypsinized and plated onto fibronectin-coated plates for 2 hr and then treated with PDGF-BB (10 ng/ml) for a further hour prior to lysis in a buffer containing 0.1% Triton X-100. myc-Rabaptin-5 was immunoprecipitated from lysates using magnetic beads conjugated to an antibody recognizing the myc-epitope. The lysates and immunoprecipitates were probed for the presence of Rabaptin-5, Cherry-Rab4/5 and PKD1 by immunoblotting.

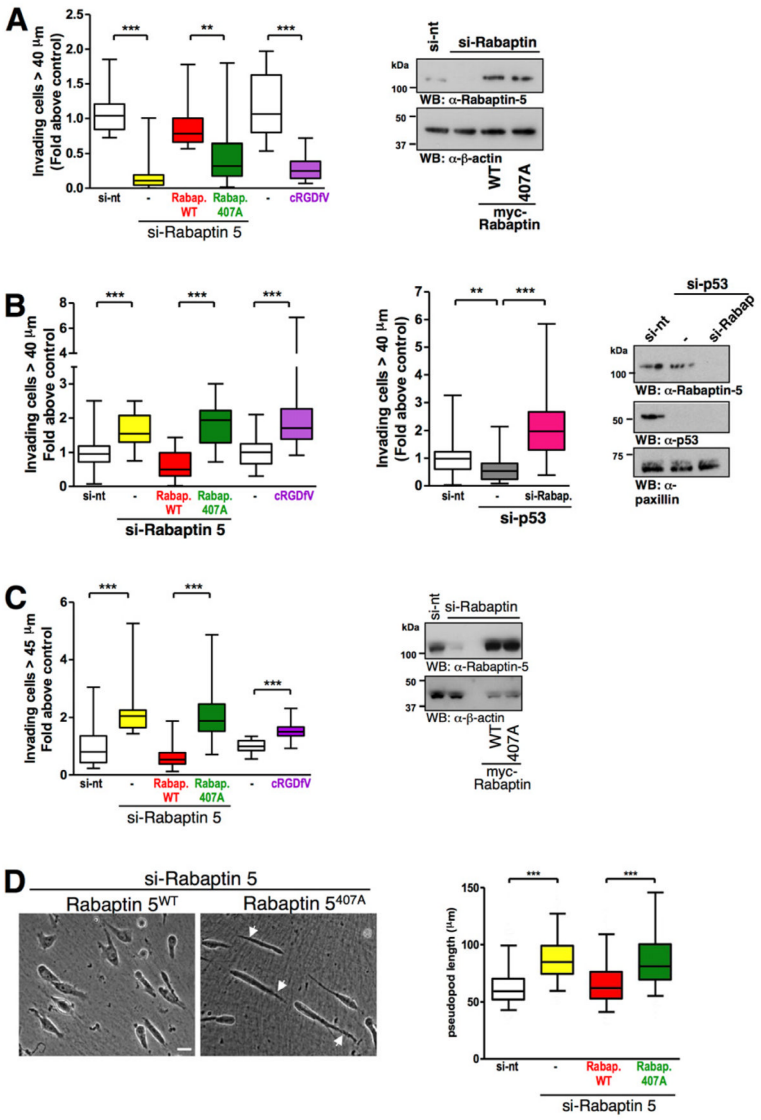

Figure 6. Rabaptin-5 phosphorylation regulates invasion and cell morphology in 3D microenvironments

(A–C) MDA-MB-231 (A,B) or A2780 (C) cells were transfected with non-targeting control siRNA (si-nt), Rabaptin-5 siRNA, or p53 siRNA without (−) or with WT or Ser407Ala Rabaptin-5. The invasiveness of transfected cells into plugs of Matrigel without (A) or with (B, C) the inclusion of fibronectin (25 μg/ml) was determined using an inverted invasion assay. cRGDfV (2.5 μM) was added to the Matrigel as indicated. Invading cells were stained with Calcein AM and visualized by confocal microscopy. Serial optical sections were captured at 10 μm or 15 μm intervals (these are presented in Figure S3 as a sequence in which the individual optical sections are placed alongside one another with increasing depth from left to right as indicated). Invasion is expressed as the proportion of cells within the plug that migrate further than 40 μm (A, B) or 45 μm (C). Data are represented as box and whiskers plots (whiskers are min to max) from three independent experiments. *** = p<0.0001; **P<0.0011 (Mann-Whitney test). Immunoblots display the knockdown and rescue of Rabaptin-5 in MDA-MB-231 (A) and A2780 (C) cells, and the Western blot in (B) shows the combined knockdown of Rabaptin-5 and mutant p53 in MDA-MB-231 cells.

(D) A2780 cells were transfected with Rabaptin-5 siRNA and rescue mutants as in (C) and plated on cell-derived matrix. Images were capture every 10 min over a period of 16.5 hr, movies were generated from these and stills from these movies are presented. White arrows indicate cells exhibiting pseudopod extension (bar, 50 μm). The length of pseudopods extended in the direction of cell migration was quantified and the data are represented as box and whiskers plots (whiskers are 5–95 percentile) from three independent experiments. *** = $p<0.0001$ (Mann-Whitney test). The box-and-whiskers plots represent: median line; box=quartiles; whiskers=min to max.